Sia Nemat-Nasser[1]
e-mail: sia@ucsd.edu

Jeom Yong Choi

Wei-Guo Guo

Jon B. Isaacs

Center of Excellence for Advanced Materials,
Department of Mechanical and Aerospace Engineering,
University of California, San Diego,
9500 Gilman Drive,
La Jolla, CA 92093-0416

Minoru Taya
Center for Intelligent Materials and Systems,
Department of Mechanical Engineering,
University of Washington, Box 352600, Seattle,
WA 98195-2600

High Strain-Rate, Small Strain Response of a NiTi Shape-Memory Alloy

The compressive response of a NiTi shape-memory alloy is investigated at various strain rates using UCSD's modified $\frac{1}{2}$-in. Hopkinson pressure bar and a conventional Instron machine. To obtain a constant strain rate during the formation of a stress-induced martensite in a Hopkinson test, a copper tube of suitable dimensions is employed as a pulse shaper, since without a pulse shaper the strain rate of the sample varies significantly as its microstructure changes from austenite to martensite, whereas with proper pulse shaping techniques a nearly constant strain rate can be achieved over a certain deformation range. The NiTi shape-memory alloy shows a superelastic response for small strains at all considered strain rates and at room temperature, 296 K. At this temperature and below a certain strain rate, the stress–strain curves of the NiTi shape-memory alloy display two regimes: an elastic austenite regime and a transition (stress-induced martensite) regime. The transition stress of this material and the work-hardening rate in the stress-induced martensite regime increase with increasing strain rate, the latter reaching a steady state level and then rapidly increasing. [DOI: 10.1115/1.1839215]

Keywords: NiTi, Shape-Memory Alloy, Strain Rate, Superelasticity, Hopkinson Bar

1 Introduction

Shape-memory alloys have been extensively studied as functional materials for a variety of applications, including medical, structural, and other advanced devices [1–8]. The understanding of their mechanical properties and their microstructural changes at various strain rates and temperatures is crucial to their proper and optimal application. The static properties of shape-memory alloys have been extensively studied. Their dynamic properties, however, have not been fully explored, especially their phase transformation at high strain-rates and their strain-rate sensitivity. The strain rate in quasi-static tests can be controlled by controlling the rate of extension independently of the resulting phase transformation [9–11]. Under quasi-static loading conditions, the applied stress during stress-induced martensite formation may be adjusted to ensure a relatively constant strain rate. However, in dynamic deformation induced by the Hopkinson pressure bar, the strain rate may change as the microstructure of the material changes, being directly related to the response of the sample. In addition, the work-hardening rate in the stress-induced martensite formation regime increases with an increasing strain rate due to the latent heat of transformation and the heat of deformation [11,12]. Ogawa [13,14] has investigated the mechanical response of shape-memory alloys over a range of initial temperatures (200 to 365 K) at 10^{-4}/s and variable high strain rates (200 to 700/s), without seeking to control the strain rate in his high strain-rate experiments. He mentions that the overall stress level in his dynamic experiments was higher than that in the quasi-static case. Recently, Chen et al. [15] have used a pulse-shaping technique to control the strain rate within the stress-induced martensite formation regime in dynamic loading. They also point out that the stress for the stress-induced martensite formation increases with an increasing strain rate in the range of 130/s to 750/s, and that the reverse transformation from the martensite to the austenite phase in dynamic deformation differs from that in the quasi-static one. Millett et al. [16] also observed a strain rate sensitivity for NiTi alloys, mentioning that the yield stress is increased from ~500 MPa at quasi-static loading to almost 800 MPa at shock loading. In addition, Liu et al. [17,18] studied the tensile deformation behavior of the thermally-induced twinned martensitic NiTi alloys at strain rates up to 300/s. They point out that the detwinning stress of the martensite is not very sensitive to the strain rate, whereas the strain-hardening effect in the dislocation deformation regime is more strongly dependent on the strain rate. These investigations all suggest the strain rate sensitivity of the stress-induced martensite formation in shape-memory alloys. The phenomenon, however, has not been fully understood due to the difficulty in controlling the corresponding strain rate.

An aim of the present work has been to examine possible pulse-shaping techniques necessary for evaluating the compressive dynamic response of a NiTi shape-memory alloy at relatively constant high strain rates, using a recovery Hopkinson pressure bar system. In this paper, we report both the quasi-static and dynamic superelastic responses of this material over a broad range of strain rates, all at 296 K initial temperature.

2 Experimental Procedure

Specimen Preparation. The composition of the material used in the present study is 50.4Ni–49.6Ti (at.%). A_f is around 296 K. Circular cylindrical samples with 5 mm nominal diameter and 5 mm nominal length are cut by electro-discharge machining (EDM). To study the superelastic response of the material, the maximum strain must be limited to no more than 8%, above which permanent plastic deformation occurs.

Low and High Strain-Rate Experiments at Room Temperature. The quasi-static compression tests are performed using an Instron hydraulic testing machine, over a range of strain rates from 10^{-4}/s to 1/s, with the maximum strain remaining within the superelastic range. The deformation of the specimen is measured by an LVDT, mounted in the testing machine and is calibrated before the test.

The dynamic compression tests are carried out using UCSD's recovery Hopkinson technique [19,20] at room temperature. Figure 1 is a schematic diagram of the split Hopkinson pressure bar, showing a striker bar, a pulse-shaping material, an incident bar, and a transmission bar. In addition, the figure shows an appropriately oriented copper-tube pulse-shaper. The specimen is sand-

[1]Corresponding author: Fax: +1-858-534-2727.

Manuscript received February 4, 2004; revision received September 23, 2004. Review conducted by: M. Cherkaoui.

Copyright © 2005 by ASME

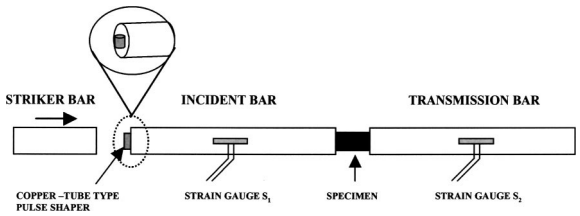

Fig. 1 Schematic diagram of the split Hopkinson bar with a pulse shaper

wiched between the incident and transmission bars. Both ends of the specimen are greased to reduce the end-friction effect on the specimen deformation during the dynamic test. A gas gun propels the striker bar towards the incident bar, to which a pulse shaper is attached, impacting the pulse shaper that transmits a compressive pulse into the incident bar. The time-variation of this transmitted pulse depends on the response of the pulse shaper and can be controlled to a certain extent by a proper choice of the pulse shaper. The elastic compressive pulse travels along the incident bar towards the specimen. A small part of the energy of the elastic pulse is transmitted through the sample into the transmission bar, and the remaining energy is reflected back into the incident bar as a tensile release pulse. Strain gauges mounted on the midpoint of the incident and transmission bars record the incident, reflected, and transmitted pulses as functions of time. The electrical signals from the strain gauges are recorded and analyzed. The stress and strain in the specimen are calculated from the transmitted (the stress) and reflected (the strain) pulses, respectively. From the reflected pulse, the time-dependent (nominal or engineering) strain rate, $\dot{\varepsilon}_S(t)$, of the sample is obtained,

$$\dot{\varepsilon}_S(t) = -\frac{2C_0}{L_S}\varepsilon_R(t), \tag{1}$$

where C_0 is the common longitudinal sound velocity of the bars, $\varepsilon_R(t)$ is the time-dependent reflected strain, and L_S is the original length of the specimen. Therefore, the strain of the sample, ε_S, is given by,

$$\varepsilon_S = -2\frac{C_0}{L_S}\int_0^t \varepsilon_R(\tau)d\tau. \tag{2}$$

The transmitted compressive pulse gives the time-dependent (nominal or engineering) stress, $\sigma(t)$, in the sample,

$$\sigma(t) = \frac{A_0}{A_S}E\varepsilon_T(t), \tag{3}$$

where $\varepsilon_T(t)$ is the time-dependent transmitted strain, A_0 is the cross-sectional area of the transmission bar (also that of the incident bar), A_S is the initial cross-sectional area of the specimen, and E is the common Young's modulus of the bars, respectively.

Pulse-Shaping Technique. For a sample to deform at a constant strain rate in a Hopkinson test, the reflected strain must be constant during the sample deformation, as is evident from Eq. (1). During the loading, the sample is subjected to the following forces:

$$F_1 = EA_0(\varepsilon_I(t) + \varepsilon_R(t)), \tag{4a}$$

$$F_2 = EA_0(\varepsilon_T(t)), \tag{4b}$$

where F_1 and F_2 are forces acting on the sample at its interface with the incident bar and transmission bar, respectively. Once the equilibrium condition, $F_1 \simeq F_2$, is attained, then the reflected pulse relates to the incident and the transmitted pulses, by

$$\varepsilon_I(t) + \varepsilon_R(t) \simeq \varepsilon_T(t). \tag{5}$$

From Eqs. (1) to (5), it follows that

$$EA_0\varepsilon_I(t) - A_s\sigma(t) \simeq \frac{L_S EA_0}{2C_0}\dot{\varepsilon}_S(t). \tag{6}$$

It is therefore seen that the sample strain rate depends on both the incident elastic pulse and the transmitted pulse that is affected by the response of the specimen. Thus, to achieve a constant strain rate, the time-variation of the incident pulse must be similar to that of the stress transmitted by the sample into the transmission bar. The flow stress of most metals increases monotonically with the strain, once yielding occurs. With an accompanying thermal softening, which takes place at high loading rates, the sample stress generally displays a small time-variation. Thus, it is often easy to produce an incident pulse of a suitable time-profile to render the resulting sample strain rate essentially constant, since the shape of the incident pulse can be controlled by adjusting the geometry and properties of the pulse shaper according to the length and velocity of the striker bar; see Nemat-Nasser et al. [19] who analyze this problem in detail and provide examples. As shown by these authors, a small copper button produces a ramped incident pulse, which is adequate to ensure a constant strain rate for most metals.

The stress–strain relation for shape-memory alloys within the superelastic range is partly concave down and partly concave up, requiring special pulse shaping in order to ensure a constant strain rate. To achieve this, several different pulse shapers were examined, and suitable copper tubes were selected, depending on the length and velocity of the striker bar. A copper tube, placed on the incident bar's end as shown in Fig. 1, can transmit a compressive pulse into the incident bar that may have the desired profile. The transmitted pulse initially is more or less flat, but becomes concave up once the tube is essentially collapsed.

3 Superelastic Response of NiTi Under Constant Strain Rate

As pointed out above, the strain rate achieved in testing a NiTi shape-memory alloy sample using a Hopkinson pressure bar is sensitive to the response of the sample and hence to the test temperature and sample stress. As a preliminary exploration, tests are performed at an initial temperature of 296 K without a pulse shaper within the superelastic range, starting with the austenitic microstructure, which then changes to stress-induced martensite during loading, gradually returning to its original austenite structure in unloading. Figure 2 is a typical strain profile as a function of time in the superelastic range. It is obtained using a 15.24 cm striker bar at about 9.7 m/s, attaining a desired 5.5% maximum strain. The slope of the strain–time curve gives the strain rate, $\dot{\varepsilon}$

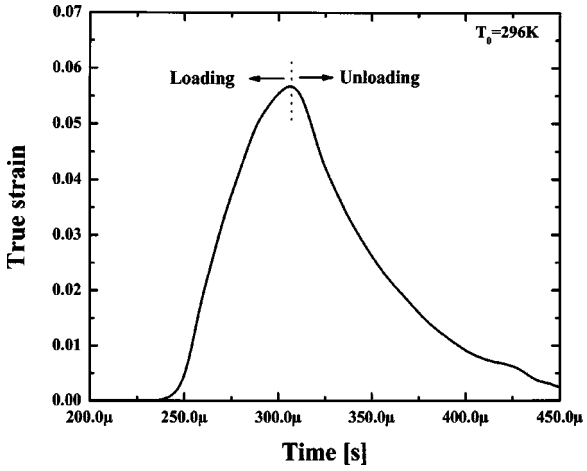

Fig. 2 Time-variation of strain without a pulse shaper

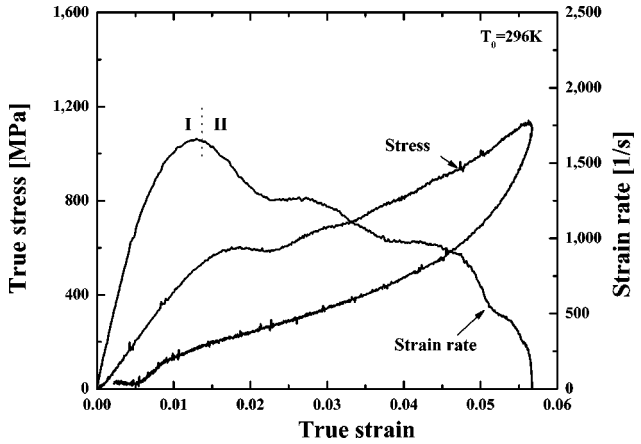

Fig. 3 Variation of stress and strain rate as a function of strain in a test without a pulse shaper

$=d\varepsilon/dt$. As is evident from Fig. 3, the strain rate is not constant during loading. Referring to Fig. 3, the strain rate is divided into an elastic regime I with austenite microstructure, and a regime II, during which phase transformation from austenite to stress-induced martensite takes place and where the strain rate begins to decrease at a roughly constant rate as stress-induced martensites are formed.

The Hopkinson bar without a pulse shaper produces a trapezoidal- or square-shaped incident pulse. With this type of incident pulse, one cannot obtain constant strain rates for shape-memory alloy samples as they undergo phase transformation. To obtain a constant strain rate, the time-dependence of the incident pulse must be similar to that of the transmitted pulse, as is evident from Eq. (6). Figure 4 compares the result obtained without a pulse shaper (Fig. 4(*a*)) with those obtained using a square copper plate containing a central hole (Fig. 4(*b*)) and a copper tube (Fig. 4(*c*)). The pulse shapers have produced similar transmitted pulses, with the square plate being better in loading but not necessarily in unloading where strain recovery takes place; this recovery for shape-memory alloys is apparently affected by the time-variation of the incident pulse. Figure 5 illustrates the variation of the stress and the instantaneous strain rate as functions of strain for the two pulse shapers, obtained using a 7.62 cm striker bar. Arrows in this figure mark the location where the strain rate begins to decrease rapidly. For the square plate with a central hole, the strain rate initially increases, and then it gradually decreases during the entire deformation regime, while the sample is still deforming. For the copper tube, on the other hand, a relatively constant strain rate is attained over a greater part of the deformation regime. We thus conclude that the copper-tube pulse shaper is preferred even though the reverse transformation is still affected by the decreasing portion of the incident pulse. Figure 6 shows the time-variation of the strain using a copper-tube pulse shaper. The overall strain rate (between the arrows in Fig. 6) is about 570/s.

The dynamic response of the NiTi shape-memory alloy is further examined by using a copper-tube pulse shaper. Figure 7 shows a typical stress–strain relation for a strain rate of about 1080/s. The response may be divided into four regimes: regime I corresponds to the elastic deformation of the sample in the austenite phase; regime II corresponds to the material's forward transformation from an austenite to a stress-induced martensite; regime III is the reverse transformation from the stress-induced martensite to an austenite; and regime IV is the elastic recovery of an austenite. Regimes I and II are the loading response of NiTi, whereas regimes III and IV are its unloading response. The transition stress, σ_{fr}^{s}, which is the critical stress for austenite to stress-induced martensite transformation, is defined by the intersection of the lines tangent to the curves in regime I and the initial portion

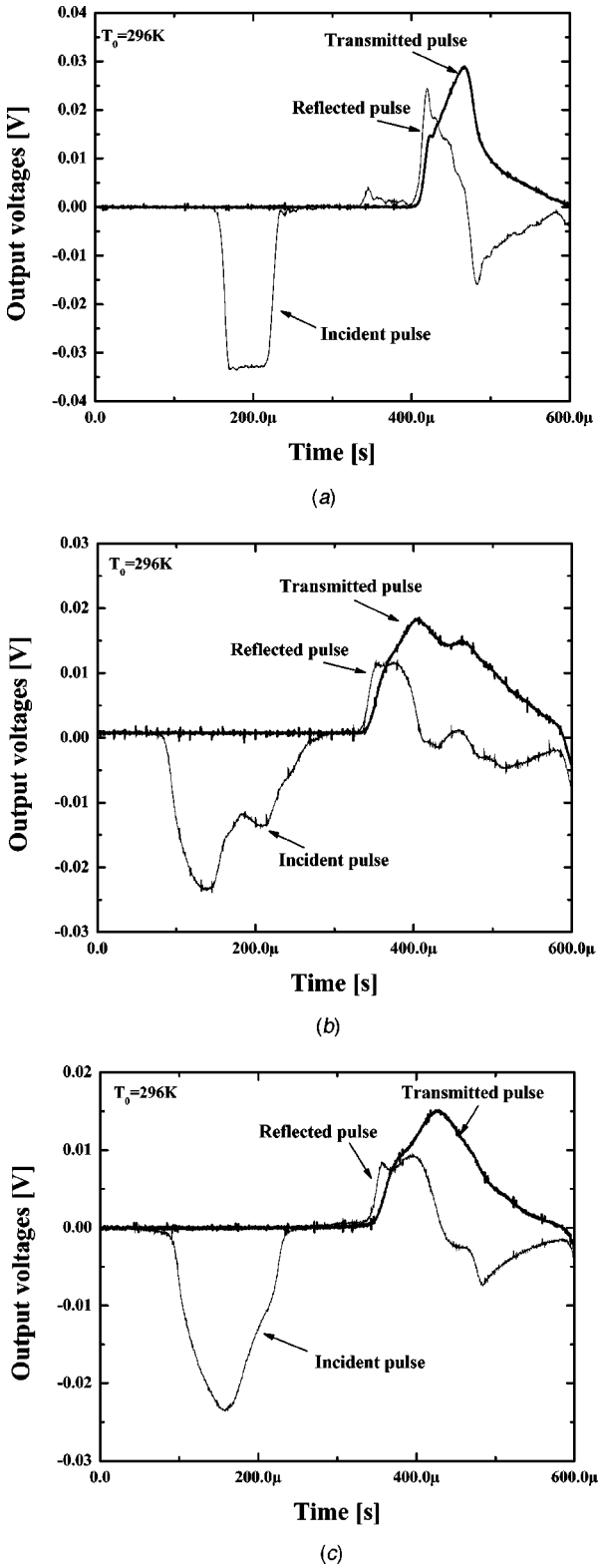

Fig. 4 A comparison of incident and transmitted pulses obtained using (*a*) no pulse shaper; (*b*) a square plate with a central hole pulse shaper; and (*c*) a tube pulse shaper

of regime II. In Fig. 7, E_1 denotes the area within the hysteresis loop, whereas E_2 denotes the area under the unloading curve. Figure 8 shows the stress–strain curves of NiTi at several indicated strain rates. The superelastic property is displayed in this figure, but the strains are not completely recovered at the instant

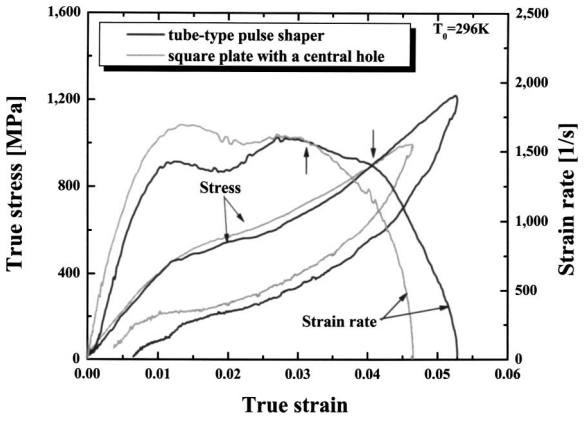

Fig. 5 Stress and strain rate as functions of strain for indicated pulse shapers

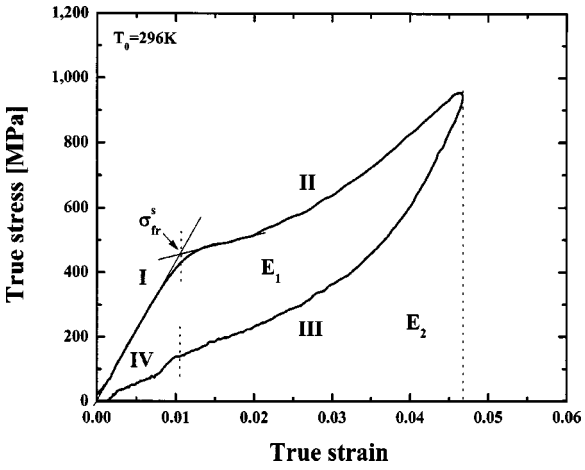

Fig. 7 A typical dynamic stress–strain relation for NiTi shape-memory alloy loaded at an average strain rate of about 1080/s

of complete unloading. Size measurement after the samples have been recovered from the testing machine, however, shows no measurable residual strains, suggesting that an additional recovery has occurred after the tests have been completed. Moreover, clear upper and lower stress plateaus, corresponding to the stress-induced martensite formation and the reverse austenite transition from martensite, are not observed in Fig. 8. Upon loading, the curves have an initially flat part (austenite phase) followed by a plateau-like portion, which begins at the transition stress, σ_{fr}^{s}, that marks the stress-induced martensite formation regime, and continues with the stress increasing upon further deformation, as is also observed by Chen et al. [15]. The material work-hardening, defined by the slope of the stress–strain curve, continues to increase with increasing fractions of the stress-induced martensite, and this hardening appears to be strain-rate dependent in the range of the considered strain rates. In unloading, the sample displays reverse transformation into an elastic return regime, but without a clear transition stress.

Two factors should be considered in examining the stress-induced martensite formation during deformation [11,12]. First, the stress-induced martensite formation is an exothermic process, leading to an increase in the temperature of the specimen. Second, at high strain rates, the generated heat remains within the specimen, increasing its temperature during deformation and phase transition. These temperature variations affect the critical stress of stress-induced martensite formation, as is suggested by the Clausius–Clapeyron equation that provides a relation between the deformation temperature and the critical stress of stress-induced martensite formation [21]. Hence, both the dynamic and thermomechanical effects may cause an increase in the stress-induced martensite formation stress. It is well known that only a small portion of the deformation work is generally stored in the material as the elastic energy of defects; see Bever et al. [22]. At high strain rates, the deformation is essentially adiabatic and the increase in the temperature of the specimen due to its deformation may be estimated using the following equation:

$$\Delta T_d = \oint \frac{\beta}{\rho \bar{C}} \sigma d\varepsilon, \tag{7}$$

where ρ is the mass density ($\rho = 6450$ kg/m^3); β denotes the fraction of the deformation work actually converted to heat ($\beta \approx 1$) [23]; $\bar{C}$ is an average heat capacity of the specimen ($\bar{C} = 500$ J/kgK); and the integration is taken over the hysteresis loop, represented by E_1 in Fig. 7. In addition, it is assumed that most of the dissipated energy is released into heat, even though the dissipated energy in the superelastic behavior of shape-memory alloys consists of two terms: heat and nonthermal energy such as sound waves and vibrations. The area of the hysteresis loop is E_1 (used in the temperature calculation), and the area under the loading curve is $E_1 + E_2$. To obtain the actual temperature increase, we must also include the latent heat, about 4.3

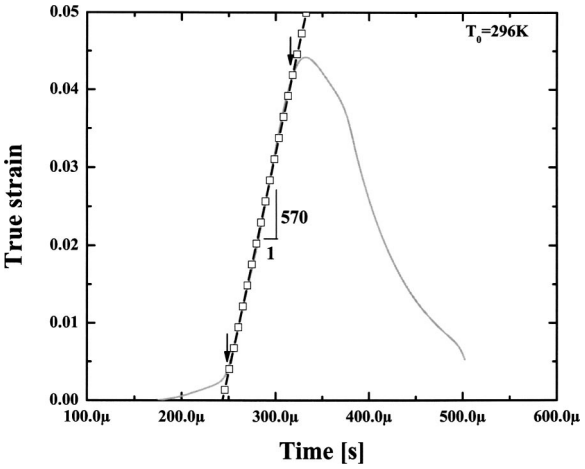

Fig. 6 Time-variation of strain, obtained using a copper-tube pulse shaper

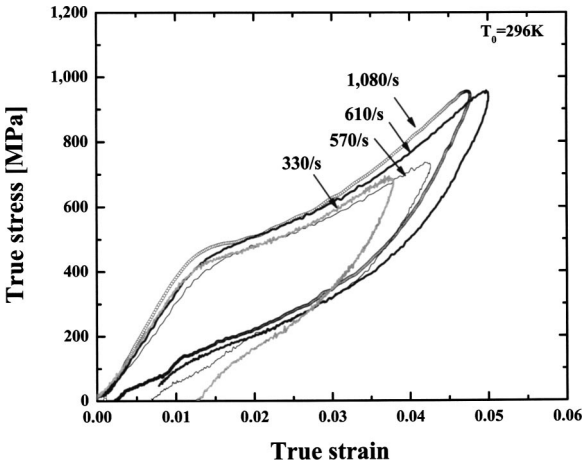

Fig. 8 Dynamic stress–strain relations for NiTi shape-memory alloy at indicated strain rates

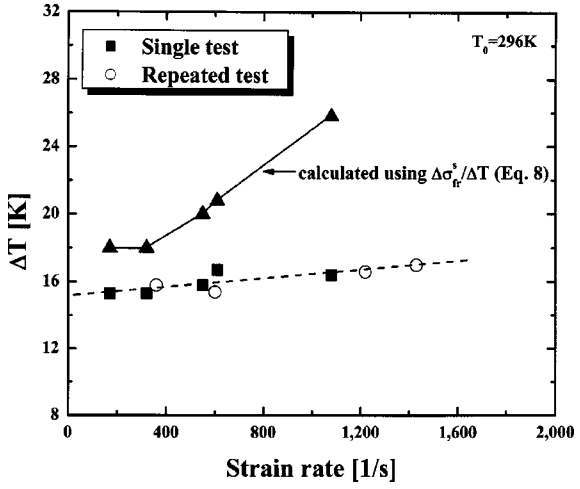

Fig. 9 Estimated temperature change as a function of strain rate; specimens denoted as a "Single Test" are loaded only once, whereas those denoted as a "Repeated Test" have been deformed several times

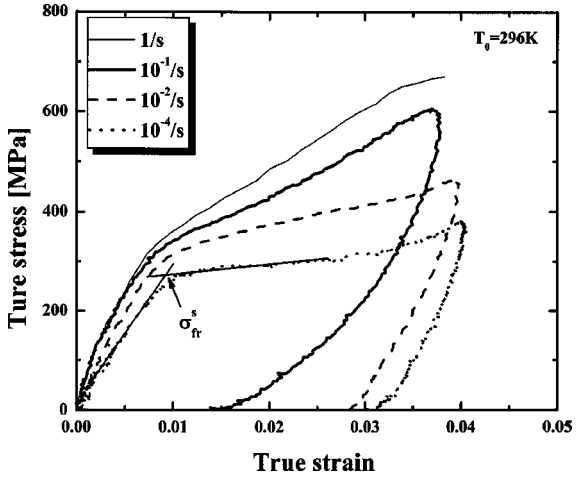

Fig. 10 Quasi-static stress–strain curves at room temperature

$\times 10^7$ J/m^3 [24], which accompanies the transformation of an austenite to a stress-induced martensite. If we assume that the austenite sample has transformed into the 100% martensite at the maximum strain, the increase of the temperature, ΔT_L, would be approximately 13 K due to the latent heat of phase transformation. Figure 9 shows the temperature rise in the specimen as a function of the strain rate calculated using both Eq. (7) and the latent heat of transformation; $\Delta T = \Delta T_d + \Delta T_L$. The calculated temperature rise under adiabatic conditions is slightly greater than that observed by McCormick et al., ~13 K [25].

We have also estimated a Clausius–Clapeyron slope for this material using a 10^{-3}/s strain rate and various initial temperatures, arriving at,

$$\frac{\Delta \sigma_{fr}^{s}}{\Delta T} = 6 \quad \text{MPa/K.} \tag{8}$$

The temperature variation calculated using Eq. (8) is also included in Fig. 9. showing a rapid increase in ΔT with increasing strain rate, in contrast with that obtained directly from the experimental results. It has been reported in the literature [10,26] that the Clausius–Clapeyron slope at low strain rates is smaller than that at a high strain rates. Therefore, calculating the temperature rise using the same Clausis–Clapeyron slope at strain rates that change by many orders of magnitude may lead to serious errors. The curves in Fig. 8 show that a higher transition stress, σ_{fr}^{s}, and a higher stress level occur at higher strain rates, resulting in greater deformation work and hence temperature increase.

4 Room Temperature Response at Low Strain Rates

Experiments are also performed at room temperature over a range of strain rates from 10^{-4}/s to 1/s, using an Instron hydraulic testing machine. The maximum strain was limited to within the superelastic range in these tests. The resulting stress–strain relations are shown in Fig. 10. The transition stress and the work-hardening rate of the material in the stress-induced martensite formation regime appear to be strain-rate dependent in this range of strain rates. As the strain rate increases, the transition stress of the stress-induced martensite formation and the work-hardening rate within the stress-induced martensite formation regime increase. Moreover, the residual strain of each test decreases with an increase of the strain rate. We did not obtain the exact unloading curve at a strain rate of 1/s, due to the dynamic response of the testing machine. An examination of this figure reveals the superelastic property even though the stress–strain curves show residual strains at zero stress. For instance, the residual strain is about 3% at a strain rate of 10^{-4}/s. A size measurement after the sample has been recovered from the testing machine shows that the residual strain has disappeared after a short time at room temperature, indicating that additional recovery has occurred after the tests have been completed, as has also been observed by Chen et al. [15]. To study the residual strain recovery, we have carefully and accurately measured the change in the residual strain at zero stress, using an accurate extensometer, in addition to the LVDT, of the testing machine. The residual strain measured by the extensometer, continues to decrease and eventually disappear, a fact that is not revealed by the LVDT due to the effect of the machine stiffness and other inaccuracies.

5 Discussion and Conclusions

It has been known that the response of NiTi shape-memory alloys is sensitive to the strain rate. At an initial room temperature and for small strain, the material displays superelasticity over a broad range of strain rates from 10^{-4}/s to 2000/s. The transition stress, which is the stress for stress-induced martensite formation, monotonically increases with an increasing strain rate; above a strain rate of around 1000/s, there is a marked increase in the stress, showing the strain rate sensitivity behavior which is similar to the flow-stress response of most ordinary metals; see Fig. 11. According to the nucleation and growth model of a martensite [27], the interface of martensite consists of coherency dislocations or misfit dislocations. The interfacial motion is of fundamental importance to the nucleation and growth of a martensite. On the basis of the dislocation model of the interfacial structure, the motion of the martensite interface is expected to be similar to that of slip dislocations. Grujicic et al. [28,29] have studied the kinetics of interface motion in a Cu–Al–Ni alloy. They suggest a thermally-activated interfacial motion model. They also mention that the mobility of a twinned martensite is greater than that of a dislocation martensite due to the weak interaction of the interface with various obstacles. This thermally-activated interfacial motion model can explain the dependence of stress on the strain rate, at strain rates below around 1000/s. However, it does not address the rapid increase of stress at a strain rate of around 1000/s. At strain rates above 1000/s, there may exist an interfacial drag effect, similar to that of dislocation slip at high strain rates. We are currently studying this strain-rate sensitivity of the flow stress, seeking to relate the interfacial motion of the stress-induced martensite to the transition stress for a stress-induced martensite.

At a very low strain-rate, however, the stress–strain curve displays a clear plateau, corresponding to the stress of stress-induced

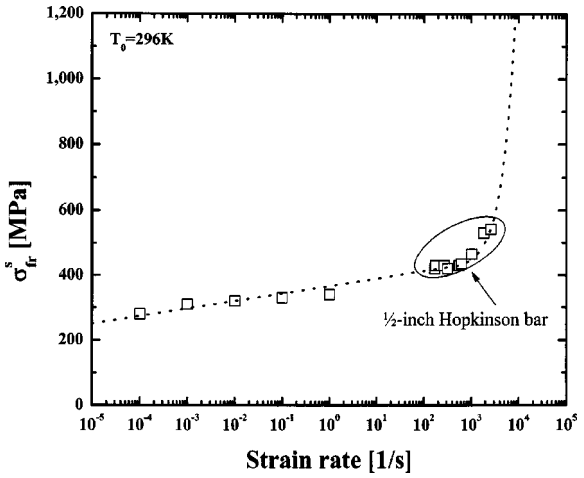

Fig. 11 Transition stress of stress-induced martensite formation as a function of strain rate

martensite formation; see Fig. 10. As the strain rate increases, the plateau slowly disappears. The stress–strain relations at moderately high strain rates are quite different when compared with those at lower strain-rates; compare Figs. 8 and 10.

The NiTi shape-memory alloy has two work-hardening rates, depending on the strain range: the stress-induced martensite formation regime and the plastic deformation regime of the resulting martensite. Figure 12 illustrates the work-hardening rate as a function of the strain rate in the stress-induced martensite formation regime. The work-hardening rate linearly increases with an increase in the strain rate until a strain rate of about 1/s is reached. Then, it remains essentially constant up to a strain rate of about 1000/s, after which it again increases with the increasing strain rate in the considered range above 1000/s. The increase in the work-hardening rate in the range of strain rates from 10^{-4}/s to 1/s during the stress-induced martensite formation, may be due to the latent heat of transformation and the heat of deformation [11,12]. However, the constant work-hardening rate in the range of strain rates from 1/s to 1000/s, and its increase for strain rates exceeding 1000/s, cannot be explained by this concept. This rapid increase in the work-hardening rate may be related to the dislocation drag effect on the interfacial motion of the stress-induced martensites.

In summary, compressive tests are performed on cylindrical samples to investigate the mechanical response of a NiTi shape-memory alloy at various strain rates and at an initial temperature of 296 K, using UCSD's modified $\frac{1}{2}$-in. Hopkinson bar and an Instron hydraulic testing machine. Several noteworthy conclusions are as follows:

1. A constant strain rate is attained during the formation of a stress-induced martensite, using the Hopkinson bar with a suitable pulse-shaping technique.
2. The NiTi shape-memory alloy shows a superelastic response for small strains at considered strain rates and at room temperature. The stress–stain curves include two regimes: an initial austenite deformation regime, and a stress-induced martensite formation regime.
3. The transition stress from the austenite to the martensite phase shows a sudden increase at around 1000/s, appearing to be strain-rate dependent in the considered strain-rate ranges. It may be related to the dislocation interfacial motion of a martensite, suggesting that at strain rates below 1000/s, the interfacial motion of a martensite is dominated by the thermally-activated motion of dislocations, and above 1000/s, by an interfacial drag effect.
4. The work-hardening rate of the stress-induced martensite formation regime linearly increases with an increase in the strain rate up to a strain rate of 1/s, and then, it remains essentially constant up to 1000/s. Beyond 1000/s, the work-hardening rate rapidly increases with the increasing strain rate.

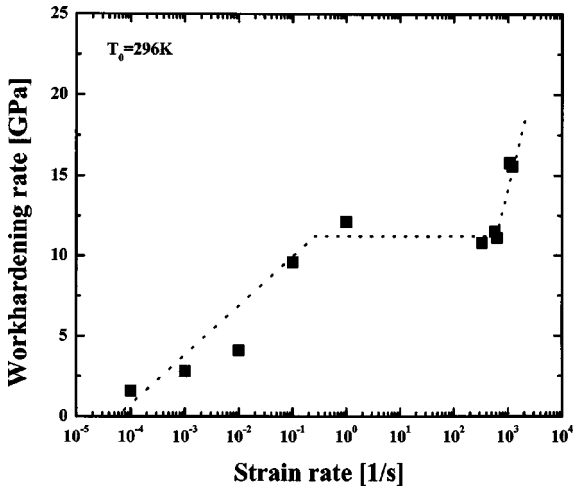

Fig. 12 Variation of the work-hardening rate with the strain rate in the stress-induced martensite formation regime

Acknowledgment

This work was supported by ONR (MURI) Grant No. N000140210666 to the University of California, San Diego.

References

[1] Otsuka, K., and Wayman, C. M., 1998, *Shape Memory Materials*, Cambridge University Press, Cambridge, UK.
[2] Van Humbeeck, J., 2001, "Shape Memory Alloys: A Material and a Technology," Adv. Eng. Mater., **3**, pp. 143–156.
[3] Dolce, M., and Cardone, D., 2001, "Mechanical Behavior of Shape Memory Alloys for Seismic Applications 2: Austenitic NiTi Wires Subjected to Tension," Int. Mech. Sci., **43**, pp. 2657–2677.
[4] Duerig, T. W., Pelton, A., and Stockel, D., 1999, "An Overview of Nitinol Medical Applications," Mater. Sci. Eng., A, **237A–275A**, pp. 149–160.
[5] Otsuka, K., and Ren, X., 1999a, "Martensitic Transformation in Nonferrous Shape Memory Alloys," Mater. Sci. Eng., A, **273A–275A**, pp. 89–105.
[6] Otsuka, K., and Ren, X., 1999b, "Recent Developments in the Research of Shape Memory Alloys," Intermetallics, **7**, pp. 511–528.
[7] Van Humbeeck, J., 1999, "Non-Medical Applications of Shape Memory Alloys," Mater. Sci. Eng., A, **237A–275A**, pp. 134–148.
[8] Otsuka, K., and Shimizu, K., 1986, "Pseudoelasticity and Shape Memory Effects in Alloys," Int. Met. Rev., **31**, pp. 93–114.
[9] Jacobus, K., Sehitoglu, H., and Balzer, M., 1996, "Effect of Stress State on the Stress-Induced Martensitic Transformation in Polycrystalline Ni–Ti alloy," Metall. Mater. Trans. A, **27A**, pp. 3066–3073.
[10] Lin, P.-H., Tobushi, H., Tanaka, K., Hattori, T., and Ikai, A., 1996, "Influence of Strain Rate on Deformation Properties of TiNi Shape Memory Alloy," JSME Int. J., **39A**, 117–123.
[11] Tobushi, H., Takata, K., Shimeno, Y., Nowacki, W. K., and Gadaj, S. P., 1999, "Influence of Strain Rate on Superelastic Behavior of TiNi Shape Memory Alloy," Proc. Inst. Mech. Eng., Part L, **213**, pp. 93–102.
[12] Shaw, J. A., and Kyriakides, S., 1995, "Thermomechanical Aspects of NiTi," J. Mech. Phys. Solids, **43**, pp. 1243–1281.
[13] Ogawa, K., 1988, "Characteristics of Shape Memory Alloy at High Strain Rate," J. Phys. C, **3**, pp. 115–120.
[14] Ogawa, K., 1991, "Dynamic Behavior of Shape Memory Material," J. Phys. IV, **C3**, pp. 215–221.
[15] Chen, W. W., Wu, Q., Kang, J. H., and Winfree, N. A., 2001, "Compressive Superelastic Behavior of a NiTi Shape Memory Alloy at Strain Rates of 0.001–750 S^{-1}," Int. J. Solids Struct., **38**, pp. 8989–8998.
[16] Millett, J. C. F., Bourne, N. K., and Gray, III, G. T., 2002, "Behavior of the Shape Memory Alloy NiTi during One-Dimensional Shock Loading," J. Appl. Phys., **92**, pp. 3107–3110.
[17] Liu, Y., Li, Y., and Ramesh, K. T., 2002, "Rate Dependence of Deformation Mechanisms in Shape-Memory Alloys," Philos. Mag. A, **82**, pp. 2461–2473.
[18] Liu, Y., Li, Y., Xie, Z., and Ramesh, K. T., 2002, "Dynamic Deformation of Shape-Memory Alloys: Evidence of Domino Detwinning?," Philos. Mag. Lett., **82**, pp. 511–517.

[19] Nemat-Nasser, S., Isaacs, J. B., and Starrett, J. E., 1991, ''Hopkinson Techniques for Dynamic Recovery Experiments,'' Proc. R. Soc. London, Ser. A, **435**, pp. 371–391.
[20] Nemat-Nasser, S., and Isaacs, J. B., 1997, ''Direct Measurement of Isothermal Flow Stress of Metals at Elevated Temperatures and High Strain Rates with Application to Ta and Ta–W Alloys,'' Acta Mater., **45**, pp. 907–919.
[21] Wollants, P., Roos, J. R., and Delaey, L., 1993, ''Thermally- and Stress-Induced Thermoelastic Martensitic Transformations in the Reference Frame of Equilibrium Thermodynamics,'' Prog. Mater. Sci., **37**, pp. 227–288.
[22] Bever, M. B., Holt, D. L., and Titchener, A. L., 1973, ''The Stored Energy of Cold Work,'' Prog. Mater. Sci., **17**, pp. 5–177.
[23] Kapoor, R., and Nemat-Nasser, S., 1998, ''Determination of Temperature Rise During High Strain Rate Deformation,'' Mech. Mater., **27**, pp. 1–12.
[24] Leo, P. H., Shield, T. W., and Bruno, O. P., 1993, ''Transient Heat Transfer Effects on the Pseudoelastic Behavior of Shape-Memory Wires,'' Acta Metall. Mater., **41**, pp. 2477–2485.
[25] McCormick, P. G., Liu, Y., and Miyazaki, S., 1993, ''Intrinsic Thermal-Mechanical Behavior Associated with the Stress-Induced Matensitic Transformation in NiTi,'' Mater. Sci. Eng., A, **167**, pp. 51–56.
[26] Tobushi, H., Shimeno, Y., Hachisuka, T., and Tanak, K., 1998, ''Influence of Strain Rate on Superelastic Properties of TiNi Shape Memory Alloy,'' Mech. Mater., **30**, pp. 141–150.
[27] Olson, G. B., and Cohen, M., 1979, ''Interface-Boundary Dislocations and the Concept of Coherency,'' Acta Metall., **27**, pp. 1907–1918.
[28] Grujicic, M., Olson, G. B., and Owen, W. S., 1982, ''Kinetics of Martensitic Interface Motion,'' J. Phys. C, **4**, pp. 173–178.
[29] Grujicic, M., Olson, G. B., and Owen, W. S., 1985, ''Mobility of Martensitic Interfaces,'' Metall. Trans. A, **16A**, pp. 1713–1722.